Long-wavelength analysis of the coupling between solidification and Soret-driven convection at positive separation ratio

Layachi Hadji
Department of Mathematics, The University of Alabama, Tuscaloosa, Alabama 35487
(Received 15 June 1992)

An investigation is made of the coupling between Soret-driven convection, at positive separation ratio, and a solid-liquid interface. This phase boundary forms upon the solidification of an upper portion of a thin layer of a dilute binary mixture that is confined between highly conducting and nearly impermeable horizontal plates. Using a long-wavelength expansion, a nonlinear evolution equation is derived that includes the coupled effects of solidification and thermosolutal convection due to the Soret effect. The validity of the derivation is found to be limited to regions, in the parameter space, that are determined as functions of the separation ratio, the Lewis number, and the thickness of the solid layer. The numerical solutions of the evolution equation show that the formation of the solid layer affects the leading-order concentration profile, and that the deviation of the interface from its planar state is weakly affected by the convective currents in the liquid. The interface morphology, however, has the same form as the convective pattern in the fluid mixture. The consideration of boundaries that are poor conductors of heat leads to a problem that is characterized by a heat-transfer Biot number γ and a mass-transfer Biot number β. The threshold values for the onset of convection are determined, and their dependence on β and γ is discussed.

PACS number(s): 47.25.Qv, 68.45.−v, 64.70.Dv, 81.10.Fq

I. INTRODUCTION

Several years ago, Dauzère [1] reported results of a very interesting experiment in which a thin liquid layer was solidified from above. Dauzère was primarily interested in freezing the convective cells that had been observed by Bénard [2]. By freezing a thin layer of warm bee's wax from its free surface, which was exposed to air, Dauzère observed that the temperature difference imposed during the cooling process initiated a convective state in the form of "up-hexagons" [3] that preceded the onset of solidification. If the cooling was allowed to slowly continue, the wax began to freeze. Solidification initiated first at the upper vertices of the hexagons where the fluid was coldest, progressed downward along the cell's sides, and finally moved inward, freezing from the top to the bottom. As the last portion of the fluid solidified, the melt below was drawn upward. The final configuration of the solidified layer had a lower surface which consisted of a periodic array of hexagonal cells with elevated centers.

The investigation of purely thermal effects on the morphology of a solid-liquid interface, which included a three-dimensional pattern selection analysis, was performed by Davis, Müller, and Dietsche [4], and Dietsche and Müller [5]. They conducted a Bénard-like experiment in which a thin layer of cyclohexane, confined between two highly conducting plates, was cooled from above at a temperature below freezing. The upper part of the layer froze, and a deformable solid-liquid interface separating the solid phase from the liquid phase appeared in the process. The dependence of the interfacial patterns on the Rayleigh number, the wave number, and the thickness of the solid layer A was investigated. Their experiments showed a subcritical polygonal pattern or a steady roll pattern at a small deviation from the critical Rayleigh number and a transition to a bimodal convective state at intermediate values of the Rayleigh number. Only unsteady roll structures persisted at high Rayleigh numbers. These experiments were performed at values of A ranging between 1 and 5. Their analytical studies resulted in a bifurcation diagram that predicted two regions of bistability. In a supercritical region, rolls and up-hexagons coexist, and in a subcritical region, up-hexagons coexist with the conductive state. A quantitative comparison of the pattern formation analysis with the experiments, however, was not possible. While the analytical study was valid for very small solid thickness, the experiments had to be carried at much thicker solid layers.

In the physically more relevant problem of the freezing of a binary mixture, an added mechanism for convective motion exists, namely, the variation of density with concentration. In this case, the solidification process involves both heat and mass flows. Since the only external control parameter that appears in this problem is the temperature difference between the top and lower plates, it seems natural to inquire about the influence of the concentration gradients, which are induced by the external temperature gradient, on the solid-liquid interface morphology. This is the so-called Soret effect which arises in a mixture as a result of the presence of a term, which is proportional to the temperature gradient, in each concentration flux. This effect is measured by the separation ratio, which is defined as the ratio of solutal density gradient to thermal density gradient. This separation ratio is positive when the induced concentration gradient enhances the destabilizing effect of the temperature gra-

 ©1993 The American Physical Society

dient and it is negative when solute distribution opposes the destabilizing effect of the temperature difference.

The phenomena of Soret-induced convection has received a lot of attention in recent years (see [6] and references therein). Much of the interest is due to the rich variety of spatial and temporal structures that can be observed experimentally near threshold. The appearance of these structures depends on the magnitude and sign of the separation ratio denoted here by S. While the sign of S can depend on the mixture used, its magnitude can be controlled externally by varying the mean temperature and concentration in the liquid. In the limit of vanishing S, the classical Rayleigh-Bénard problem with infinitely conducting plates is obtained. For large S, compositional effects dominate and the Soret regime is obtained. An interesting feature of this regime is its similarities with the Rayleigh-Bénard problem with poorly conducting plates. In the first regime, two-dimensional rolls are the only stable form of convection, while in the second one, convection in the form of square patterns is preferred. Moses and Steinberg [7] and Clune and Knobloch [8] have taken advantage of this fact to study the transition between rolls and squares by varying the magnitude of the positive separation ratio S.

In previous work by Zimmermann [9] and Zimmermann, Müller, and Davis [10], an experimental investigation combined with a linear stability analysis was undertaken to investigate the coupled effects of Soret-induced convection and solidification. Using mixtures of ethyl alcohol and water, they limited their experimental study to the case of negative separation ratio. The mixture is then subject to time-dependent convection. However, they find that the presence of a solid-liquid interface forces a transition to a steady, hexagonal convection pattern from a traveling-wave pattern. For a mixture having a positive separation ratio, Hadji and Schell [11] performed a small-amplitude stability analysis on the interfacial convective patterns that form due to the coupling of Soret-driven convection and the interfacial deformations. They have predicted that down-hexagons are generally preferred, and in a small range of Rayleigh numbers, there is exchange of stabilities between squares and down-hexagons. They have also found hysterectic transitions between the static state and hexagons and between squares and hexagons. The recent experimental observations [10], even though valid for $S<0$, seem to corroborate the findings in [11] that the coupling between Soret-driven convection and the deformations of the solid-liquid interface yields a flow pattern that consists of down-hexagons. Indeed, for a thin solid layer, Zimmermann, Müller, and Davis [10] have observed an interface that consists of ice regions surrounded by ice-free regions. For a pure substance, however, the coupling between thermal convection and interface deformations induces a pattern of up-hexagons [4,5]. This will correspond to an interface consisting of ice-free regions surrounded by ice regions.

In the following analysis, the small-amplitude assumption made in Ref. [11] is relaxed, and a nonlinear evolution equation that is valid for larger deviation of the control parameter from its critical value is derived. This equation describes the asymptotic behavior of a scaled concentration. The deviation of the interface from its planar state is found to be related to the concentration and temperature perturbations. Besides the Rayleigh, Prandtl, and Lewis numbers, the separation ratio, the amount of solidification (measured by the solid layer thickness), and the dependence of the freezing temperature on composition (measured by the liquidus slope) appear as important parameters in the problem formulation. The effects of these parameters as well as those of the boundary conditions appear in the various coefficients of the evolution equation. Solutions for some values of these parameters are obtained numerically, and their influence on the shape of the interface is determined. These solutions are required to clarify further the coupling between convective currents in the liquid-phase and the solid-liquid morphology. These requirements are the primary motivations in this paper.

The remainder of the paper is outlined in the following. In Sec. II, the mathematical formulation of the problem as well as the required assumptions used in the solution are presented. The derivation of the nonlinear equation is described in Sec. III. An expression is also obtained that reveals the range in the physical parameter space for which this analysis is valid. In Sec. IV, we solve the equation numerically for some values of the solid thickness, the separation ratio, the Lewis number, and the liquidus slope; and some concluding remarks are presented in Sec. V.

II. MATHEMATICAL FORMULATION

The system we consider, in which a solid-liquid interface forms during the solidification of a dilute binary mixture with a positive separation ratio, is briefly described in this section (see [4,10] for details). The interface separating the two phases is assumed to be a surface with zero thickness through which there is transfer of heat.

A. Basic equations

We consider a thin layer of a dilute binary fluid contained between two *nearly* impermeable [12] and perfectly conducting plates that are separated by the distance d. The temperatures T_0 and T_1 are maintained at the lower and upper boundaries, respectively. The temperature gradient T_0-T_1 is selected so as to allow for the solidification of an upper portion of the fluid layer. The interface that separates the lower liquid phase from the upper solid phase is assumed to be *planar* in the static state but deformable under the influence of convective currents. (The assumption of a planar interface is discussed in Sec. V.) The assumption of boundaries that are impermeable to mass flow implies the vanishing of the flux condition $[\partial(D_s C_L + D_l T_L)/\partial z]=0$ at $z=0$ and d, where $D_l = S_T C_L (1-C_L) D$, and S_T is the Soret coefficient [13]. We ignore the variation of D_l with concentration so that the basic concentration profile is linear in the vertical coordinate. Furthermore, we neglect the changes in the concentration of the mixture that are associated with solute rejection or incorporation during the

solid formation.

The static steady state is then defined by the following:

$$T_L(z)=\frac{\Delta T}{h_l}z+T_0\ ,\quad 0\le z\le h_l \tag{2.1a}$$

$$C_L(z)=-\frac{D_l}{D_s}\frac{\Delta T}{h_l}(z-h_l)+\frac{C_s}{K}\ ,\quad 0\le z\le h_l \tag{2.1b}$$

$$C_S(z)=C_s\ ,\quad h_l\le z\le d \tag{2.1c}$$

$$\hat{T}_S(z)=\frac{T_1-mC_s/K-T_S}{h_s}(z-d)+T_1\ ,\quad h_l\le z\le d\ , \tag{2.1d}$$

where the subscripts L and S stand for liquid and solid phase, respectively. The other symbols that appear in Eqs. (2.1a)–(2.1d) are as follows: m is the slope of the liquidus line; K is the distribution coefficient, with $K\approx 1$ for consistency with our assumptions; h_s is the thickness of the solid layer; and D_s and D_l are the solute diffusion coefficient in the liquid phase and the thermal diffusion coefficient resulting from the Soret effect, respectively. The temperature difference $\Delta T=mC_s/K+T_S-T_0$, where T_S is the freezing temperature of the pure solvent and $\hat{T}_S$ is the temperature in the solid phase. In order to couple the interface corrugations to the concentration in the liquid phase, we have *supposed* that the following holds at the interface:

$$T(\eta)=mC(\eta)+T_S\ . \tag{2.2}$$

Equation (2.2) relates the freezing temperature of the mixture to its composition, and ignores the capillarity effects. The thickness of the solid layer is specified by the external boundary conditions [4],

$$A=\frac{h_s}{h_l}=\frac{T_1-T_S-mC_s/K}{T_S-T_0+mC_s/K}\ . \tag{2.3}$$

Using the Boussinesq approximation, we obtain the following dimensionless description for the temporal and spatial evolution for the velocity vector $\mathbf{v}$ and for the deviations Θ and c of the temperature and concentration distributions from the static state respectively [14]:

$$P^{-1}\left[\frac{\partial}{\partial t}+\mathbf{v}\cdot\nabla\right]\mathbf{v}=-\nabla p+R(\Theta+Sc)\mathbf{k}+\nabla^2\mathbf{v}\ , \tag{2.4a}$$

$$\left[\frac{\partial}{\partial t}+\mathbf{v}\cdot\nabla\right]\Theta=\mathbf{v}\cdot\mathbf{k}+\nabla^2\Theta\ , \tag{2.4b}$$

$$\left[\frac{\partial}{\partial t}+\mathbf{v}\cdot\nabla\right]c=\mathbf{v}\cdot k+\tau\nabla^2(c-\Theta)\ , \tag{2.4c}$$

$$\nabla\cdot\mathbf{v}=0\ . \tag{2.4d}$$

The liquid height in the static state h_l and h_l^2/κ have been used as scales for length and time, respectively. The concentration is scaled by the Soret-induced concentration gradient that exists between the lower plate and the planar interface when the system is in the static state, while temperature is scaled by (T_0-T_a), where T_a is the actual temperature at the solid-liquid interface. In the static state, T_a is approximated by mc_I+T_S, where m is the slope of the liquidus curve in the mixture's phase diagram and c_I is the solute concentration at the solid-liquid interface.

The four dimensionless parameters appearing in Eqs. (2.4) are the Rayleigh number $R=\alpha_T g h_l^3(T_0-T_a)/\nu\kappa$, the Prandtl number $P=\nu/\kappa$, the Lewis number $\tau=D_s/\kappa$, and the separation ratio $S=\alpha_s'\Delta C/\alpha_T(T_0-T_a)$. Here α_T and α_s' are the thermal and solutal expansivities, respectively, g is the gravitational constant, and ν is the kinematic viscosity. The unit vector $\mathbf{k}$ is directed opposite to the gravity vector. Only heat conduction is considered in the solid phase and this is described by the equation

$$\frac{\partial}{\partial t}\hat{\Theta}=\nabla^2\hat{\Theta}\ , \tag{2.5}$$

where $\hat{\Theta}$ is the dimensionless temperature deviation from the basic distribution in the solid phase.

The continuity equation (2.4d) can be eliminated by using the general representation for a solenoidal vector field [15]

$$\mathbf{v}=\nabla\times(\nabla\times\psi\mathbf{k})+\nabla\times\sigma\mathbf{k}\ . \tag{2.6}$$

If we take the vertical component of the curl of Eq. (2.4a), we obtain an equation for the vertical component of the vorticity σ,

$$P^{-1}\left[\frac{\partial}{\partial t}(\nabla_H^2\sigma)-\mathbf{k}\cdot\nabla\times(\mathbf{v}\cdot\nabla\mathbf{v})\right]=\nabla^2(\nabla_H^2\sigma)\ , \tag{2.7}$$

and the vertical component of the double curl of Eq. (2.4a) yields an equation for ψ,

$$P^{-1}\left[\frac{\partial}{\partial t}\nabla^2(\nabla_H^2\psi)+\mathbf{k}\cdot\nabla\times(\nabla\times\mathbf{v}\cdot\nabla\mathbf{v})\right]=\nabla^4(\nabla_H^2\psi)-SR\nabla_H^2\phi-R(1+S)\nabla_H^2\Theta\ . \tag{2.8}$$

In writing Eqs. (2.7) and (2.8), we have made use of the representation (2.6) everywhere, but omitted it in the terms containing $\mathbf{v}\cdot\nabla\mathbf{v}$ for reasons of space. Finally, the heat and the scaled concentration equations become

$$\frac{\partial\Theta}{\partial t}+\nabla_H D\psi\cdot\nabla_H\Theta-\nabla_H^2\psi D\Theta+\frac{\partial\Theta}{\partial x}\frac{\partial\sigma}{\partial y}-\frac{\partial\sigma}{\partial x}\frac{\partial\Theta}{\partial y}+\nabla_H^2\psi=\nabla^2\Theta\ , \tag{2.9}$$

$$\frac{\partial\phi}{\partial t}+\nabla_H D\psi\cdot\nabla_H\phi-\nabla_H^2\psi D\phi+\frac{\partial\phi}{\partial x}\frac{\partial\sigma}{\partial y}-\frac{\partial\sigma}{\partial x}\frac{\partial\phi}{\partial y}=\tau\nabla^2\phi-\nabla^2\Theta\ , \tag{2.10}$$

where $\phi=c-\Theta$, ∇_H is the horizontal gradient, and $D=\partial/\partial z$.

B. Boundary conditions

The complete formulation of the problem is specified by Eqs. (2.5) and (2.7)–(2.10) and appropriate boundary conditions. These boundary conditions are now briefly

introduced [10,11]. The conservation of solute at the interface located at $z=\eta(x,y,t)$ gives

$$\hat{\mathbf{N}}\cdot\nabla\phi=0 \ . \tag{2.11a}$$

The continuity of temperature and the assumption of thermodynamic equilibrium at the interface imply

$$\frac{1-\delta}{1+\delta}\Theta(\eta)-\frac{\delta}{1+\delta}\phi(\eta)=\eta-1 \tag{2.11b}$$

and

$$\Theta(\eta)=A\hat{\Theta}(\eta) \ , \tag{2.11c}$$

where $\delta=mD_l/D_s$ is the dimensionless liquidus slope [11]. The balance between the latent heat release and the jump in the heat flux at the interface yields

$$\hat{\mathbf{N}}\cdot\nabla(A\hat{\Theta}-\Theta)=0 \ . \tag{2.11d}$$

For a *nearly* impermeable lower boundary we obtain a radiation boundary condition [12]

$$D\phi(0)=\beta\phi(0) \ , \tag{2.11e}$$

where β is the mass transfer Biot number.

For top and lower plates that are infinitely conducting, we have

$$\Theta(0)=0 \ , \tag{2.11f}$$

$$\hat{\Theta}(1+A)=0 \ . \tag{2.11g}$$

The assumption of a no-slip boundary condition on the velocity at the rigid plates and at the interface, combined with mass conservation at the interface, implies

$$\psi=D\psi=0 \quad \text{at } z=0,\eta \ , \tag{2.11h}$$

$$\sigma=0 \quad \text{at } z=0,\eta \ . \tag{2.11i}$$

The unit vector $\hat{\mathbf{N}}$ in Eqs. (2.11a) and (2.11d) is normal to the interface and is given by

$$\hat{\mathbf{N}}=(-\eta_x,-\eta_y,1)/(1+\eta_x^2+\eta_y^2)^{1/2} \ . \tag{2.12}$$

Several assumptions have been made in deriving the above governing equations and boundary conditions. We have neglected any variations in the thermal diffusivity, density, and thermal conductivity of the mixture upon solidification. Furthermore, since the time scale resulting from the growth velocity is very large in comparison to the time scale of convection, the effects associated with the latent heat are ignored. Therefore, in this limit of stationary interface, changes in concentration occur over a length scale $l_c\sim D_s/V$, where V is the interface velocity, and since $l_c\gg h_l$, the convective effects are more important. From boundary condition (2.11b), we observe that for the case $\delta=0$, which corresponds to an interfacial temperature that is independent of concentration, the interface shape is determined solely by the temperature perturbation. However, when $\delta\neq 0$, the coupled concentration and temperature effects contribute in the determination of the interface morphology. In the limit of a stationary interface, and zero solute diffusion in the solid, the concentration gradients that develop at the interface are due to the convective motion in the liquid. Consequently, in order for these gradients to be felt by the interface, the concentration boundary layer that forms at the interface, due to the no-slip condition, is required to be infinitely thin. Since $|\delta|\ll 1$, we adopt the scaling $\delta=O(\epsilon^2)$, where ϵ is a small perturbation parameter which is defined in the next section, thus allowing for the effects that are due to the dependence of the interfacial temperature on composition to appear in the leading-order expression for the interface.

III. DERIVATION OF AN EVOLUTION EQUATION FOR THE INTERFACE

For a positive separation ratio, the principle of exchange of stabilities holds. Furthermore, it is known [14] that in the limit of a vanishing Biot mass-transfer coefficient β, which corresponds to the case of an impermeable boundary, and for a large positive separation ratio, the primary instability is to a long wavelength. In this paper, we are considering a system that is nearly but not completely impermeable. In this case, $\beta\ll 1$ but not zero, therefore the convective state is not homogeneous, but cellular. Proceeding along standard lines [16], we derive an evolution equation for the leading-order contribution to ϕ. We introduce the slow variables

$$(x,y)=(X,Y)/\epsilon \ , \quad t=T/\epsilon^4 \ , \quad 0<\epsilon\ll 1 \tag{3.1}$$

and expand all convective quantities, including the interface in powers of ϵ^2,

$$[\Theta,\phi,\hat{\Theta},\psi,\sigma]=[\Theta_0,\phi_0,\hat{\Theta}_0,\psi_0,\sigma_0]+\epsilon^2[\Theta_2,\phi_2,\hat{\Theta}_2,\psi_2,\sigma_2]+\cdots \ , \tag{3.2a}$$

$$\eta=1+\epsilon^2\eta_2+\cdots \ . \tag{3.2b}$$

The Rayleigh number and the mass-transfer Biot numbers are scaled as

$$R=R_0+\mu\epsilon^2+\cdots \ , \quad \mu=O(1) \ , \quad \beta=\epsilon^4\hat{\beta} \ , \quad \hat{\beta}=O(1) \ . \tag{3.3}$$

By substituting the horizontal and temporal scalings, Eq. (3.1), into Eqs. (2.5) and (2.7)–(2.10) and boundary conditions Eqs. (2.11a)–(2.11i), and by making use of the expansions, Eqs. (3.2) and (3.3), we obtain a hierarchy of boundary-value problems of different orders in ϵ that can be solved in a successive manner.

Equations (2.5), (2.9), and boundary conditions (2.11c), (2.11f), and (2.11g) give

$$D^2\Theta_0=D^2\hat{\Theta}_0=0 \ , \tag{3.4a}$$

subject to the end conditions

$$\Theta_0(0)=\hat{\Theta}_0(1+A)=0 \ , \tag{3.4b}$$

$$\Theta_0(1)=\hat{\Theta}_0(1) \ , \quad D\Theta_0(1)=D\hat{\Theta}_0(1) \ . \tag{3.4c}$$

The problem defined by Eqs. (3.4) yields the trivial solutions

$$\Theta_0=\hat{\Theta}_0=0 \tag{3.5}$$

for the leading-order contributions to the temperature

profiles of the liquid and solid phase, respectively. In writing Eqs. (3.4b) and (3.4c), we have made the transformation, $A\hat{\Theta}=\hat{\Theta}_{\text{new}}$, then dropped the subscript new.

Equations (2.10), (2.11a), and (2.11e) imply

$$D^2\phi_0=0 \quad \text{with } D\phi_0(0)=D\phi_0(1)=0 , \tag{3.6}$$

and yield the expression $\phi_0=f(X,Y,T)$ for the leading-order contribution to the concentration. Similarly, Eqs. (2.8) and (2.11h) imply

$$D^4\psi_0-SR_0\phi_0-R_0(1+S)\Theta_0=0 , \tag{3.6a}$$

subject to the boundary conditions

$$\psi_0=D\psi_0=0 \quad \text{at } z=0,1 . \tag{3.6b}$$

The solution to the boundary value problem (3.6) is

$$\psi_0=R_0Sf(z^4-2z^3+z^2)/24 . \tag{3.7}$$

We complete the solution to the leading-order problem by solving for the vorticity

$$D^2\sigma_0=0 \quad \text{with } \sigma_0(0)=\sigma_0(1)=0 \tag{3.8}$$

to find

$$\sigma_0=0 . \tag{3.9}$$

From Eqs. (2.10) and (2.11a) and (2.11e) to order ϵ^2 we obtain

$$\tau D^2\phi_2+\tau\nabla_H^2 f-\nabla_H^2\psi_0=\nabla_H D\psi_0\cdot\nabla_H f . \tag{3.10a}$$

The corresponding boundary conditions are

$$D\phi_2=0 \quad \text{at } z=0,1 . \tag{3.10b}$$

A solution of the inhomogeneous problem (3.10) exists if a solvability condition is satisfied. In this case it suffices to integrate Eq. (3.10a) over the liquid layer thickness. We thus find the critical value of the Rayleigh number for the onset of convection to be

$$R_0=720\tau/S . \tag{3.11}$$

Hence the threshold value for the onset of convection is not affected by the formation of the solid. This is not the case, however, if solute diffusion is included. By taking into account solute diffusion in the solid phase, the boundary condition on ϕ_2 at the interface, Eq. (3.10b), is replaced by a radiation boundary condition with a Biot number that depends on the thickness of the solid layer. This thickness will then appear in the expression for R_0 (see [4]).

Straightforward solution of the problem (3.10) yields

$$\phi_2=\tfrac{1}{2}(2z^6-6z^5+5z^4-z^2)\nabla_H^2 f + (6z^5-15z^4+10z^3)|\nabla_H f|^2+K . \tag{3.12}$$

where K is an integration constant which does not enter in the present calculations to the order at which they are considered. The solution to the order ϵ^2 of Eq. (2.5) that satisfies the boundary condition (2.11g) is given by

$$\hat{\Theta}_2=C[z-(1+A)] , \tag{3.13}$$

where C is an integration constant. Application of the conditions (2.11c) and (2.11d) yield

$$\Theta_2(1)=-CA \tag{3.14a}$$

and

$$D\Theta_2(1)=C . \tag{3.14b}$$

The last two equations can be combined to form a radiation boundary condition for Θ_2 at $z=1$

$$\Theta_2+AD\Theta_2=0 . \tag{3.15}$$

The order ϵ^2 of Eq. (2.9) with boundary conditions Eqs. (2.11f) and (3.15) yields

$$\Theta_2=\frac{\tau}{2}\left[2z^6-6z^5+5z^4-\frac{1+2A}{1+A}z\right]\nabla_H^2 f . \tag{3.16}$$

The matching of the second-order terms in ϵ in Eq. (2.8) and boundary conditions Eq. (2.11h) yield the following for $\psi_2(' \equiv D)$:

$$D^4(\nabla_H^2\psi_2)+2D^2(\nabla_H^4\psi_0)-SR_0\nabla_H^2\phi_2 -S\mu\nabla_H^2\phi_0-R_0(1+S)\nabla_H^2\Theta_2 =P^{-1}[2D\{(G')^2F_1+GG''F_2\}-D^2(GG')F_3] , \tag{3.17}$$

where

$$G(z)=30\tau(z^4-2z^3+z^2) , \tag{3.18}$$

$$F_1=f_{XY}^2+f_{YY}^2+f_{XX}^2-f_{XX}f_{YY} , \tag{3.19}$$

$$F_2=f_Yf_{XXY}-f_Yf_{YYY}+f_Xf_{XXX}-f_Xf_{XYY} , \tag{3.20}$$

$$F_3=(\nabla_H^2 f)^2-\nabla_H f\cdot\nabla_H(\nabla_H^2 f) . \tag{3.21}$$

The corresponding boundary conditions are

$$\psi_2(0)=D\psi_2(0)=\psi_2(1)=0 . \tag{3.22}$$

At the interface, the order ϵ^2 of Eq. (2.11h) yields

$$D\psi_2(1)=-\eta_2D^2\psi_0(1) . \tag{3.23}$$

The solution of Eq. (3.17) with boundary conditions Eqs. (3.22) and (3.23) is

$$\nabla_H^2\psi_2=\frac{1}{42S}\left\{6Wz^{10}-30Wz^9+45Wz^8-126S\tau z^6+[252S\tau-126(S+1)U\tau^2]z^5-210S\tau z^4\right.$$
$$+\left[70\frac{1+2A}{1+A}S^2\tau^2+\frac{752A+430}{1+A}S\tau^2+\frac{612A+360}{1+A}\tau^2-60S\tau\right]z^3$$
$$\left.+\left[\frac{1+2A}{1+A}S^2\tau^2+\frac{983A+535}{1+A}S\tau^2+\frac{843A+465}{1+A}\tau^2+3S\tau\right]z^2\right\}\nabla_H^4 f$$
$$+\frac{\tau}{7}[10z^9-45z^8+60z^7+100z^3-75z^2]\nabla_H^2|\nabla_H f|^2+G(z)[\nabla_H^2 K+(\mu/720)\nabla_H^2 f]$$
$$+\frac{\tau^2}{7P}[G_1(z)F_1+G_2(z)F_2-G_3(z)F_3]-[60z^3+30z^2]\nabla_H^2(\eta_2 f)\ . \tag{3.24}$$

The symbols that appear in Eq. (3.24) are defined as follows:

$$W=(S+1)\tau^2+S\tau\ , \tag{3.25a}$$
$$U=(1+2A)/(1+A)\ , \tag{3.25b}$$
$$G_1(z)=[400z^9-1800z^8+3120z^7$$
$$-2520z^6+840z^5-40z^3]\ , \tag{3.25c}$$
$$G_2(z)=[300z^9-1350z^8+2280z^7-1680z^6$$
$$+420z^5-60z^3-30z^2]\ , \tag{3.25d}$$
$$G_3(z)=[350z^9-1575z^8+2700z^7-2100z^6$$
$$+630z^5-20z^3+15z^2]\ . \tag{3.25e}$$

Finally, at order ϵ^2, Eq. (2.7) with boundary conditions Eqs. (2.11i) yields

$$\nabla_H^2\sigma_2=[30z^7-105z^6+147z^5-105z^4-2z]$$
$$\times[f_{XXX}f_Y+f_{XYY}f_Y-f_{XXY}f_X-f_{YYY}f_X]\ . \tag{3.26}$$

The boundary conditions for ϕ_4 are obtained from Eqs. (2.11a) and (2.11e),

$$D\phi_4(0)=\hat{\beta}f\ ,\quad D\phi_4(1)=\nabla_H\eta_2\cdot\nabla_H f\ . \tag{3.27}$$

Finally, the solvability requirement for ϕ_4 in the order ϵ^4 of Eq. (2.10) yields the sought evolution equation for $f(X,Y,T)$:

$$\frac{\partial f}{\partial T}=-\tau\chi(S,A,\tau)\nabla_H^4 f-(\mu\tau/R_0)\nabla_H^2 f+\nabla_H\eta_2\cdot\nabla_H f-\hat{\beta}f$$
$$+\tfrac{10}{7}\tau[\nabla_H f\cdot\nabla_H|\nabla_H f|^2+\nabla_H^2 f|\nabla_H f|^2]$$
$$-\frac{A\tau^2}{2(1+A)}[\nabla_H f\cdot\nabla_H(\nabla_H^2 f)+(\nabla_H^2 f)^2]$$
$$-15\nabla_H^2(\eta_2 f)\ , \tag{3.28}$$

where

$$\chi(S,A,\tau)=\left[\frac{17}{462}+\frac{25(1+S)\tau}{231S}-\frac{(1+S)(1+2A)\tau}{4S(1+A)}\right]\ . \tag{3.29}$$

We observe that Eq. (3.28) ceases to be well posed when the coefficient χ becomes negative. It is known that the ill posedeness of the evolution equation is due to the fact that the limit $\chi\to 0+$ is associated with an increase in the critical wave number [12,17]. These shorter wavelengths cannot be tested within the limits of this analysis. Thus the analysis presented in this paper is valid for parameters A, S, and τ for which χ is positive. The regions where the derived evolution equation, Eq. (3.28), is valid are depicted in Fig. 1, where S' is plotted against A for $\tau=0.001$, 0.005, and 0.01. The variation of S' with A is certainly expected for the present boundary conditions. While larger positive values of S favor primary instabilities with very long wavelength, increases in A have the opposite effect, in agreement with Fig. 3 of Ref. [11]. Therefore larger values of the solid thickness require larger values of the separation ratio S in order to keep the critical wave number small and the expansion consistent. For A fixed, the lower bound on S, which is required to make $\chi>0$, increases with increasing values of the Lewis number τ.

The leading-order deviation η_2 of the interface from its planar state is derived from Eq. (2.11b). We let $\delta=O(\epsilon^2)$ to allow for the coupling effects between ϕ_0 and the interfacial deformations. For $m<0$, we set $\delta=-\epsilon^2\zeta$, where

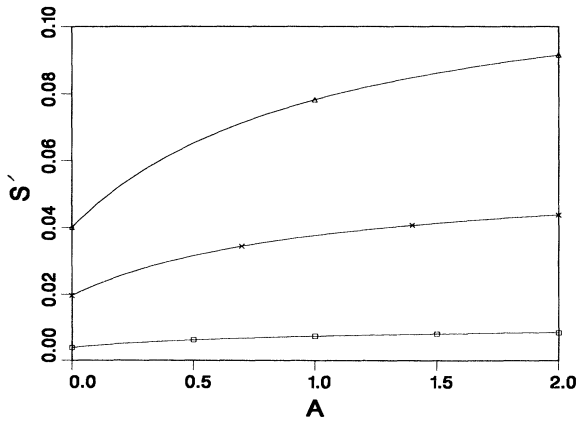

FIG. 1. Plot of the lower bound S' as a function of A for $\tau=0.001(\square)$, $\tau=0.005(\times)$, and $\tau=0.01(\triangle)$. The validity of the analysis is limited to the regions $S>S'$.

$\zeta = O(1)$, to obtain

$$\eta_2 = \frac{-\tau A}{2(1+A)} \nabla_H^2 f + \zeta f \ . \tag{3.30}$$

In the next section, we will study Eq. (3.28), restricting the analysis to two-dimensional patterns.

IV. ANALYSIS OF THE EVOLUTION EQUATION

If we eliminate the y dependence in f, and consider the following scaling:

$$w = (4\tau/\chi)T, \quad \xi = \sqrt{2/\chi}X, \quad f = \sqrt{7\chi/10}F \ , \tag{4.1}$$

then upon substitution of Eq. (3.30) for η_2, Eq. (3.28) reduces to

$$\begin{aligned} \frac{\partial F}{\partial w} = & -F_{\xi\xi\xi\xi} - 2F_{\xi\xi} - \hat{\beta}F + (F_\xi^3)_\xi \\ & - \Gamma_1 (F_\xi F_{\xi\xi})_\xi - \Gamma_2 (F_\xi F_{\xi\xi\xi}) - 5\Gamma_2 (F F_{\xi\xi})_\xi \\ & + \Gamma_3 (F_\xi^2) + 5\Gamma_3 (F^2)_{\xi\xi} \ , \end{aligned} \tag{4.2}$$

where

$$\Gamma_1 = \frac{\tau A}{2(1+A)} \sqrt{7/10\chi}, \quad \Gamma_2 = \Gamma_1/\tau, \quad \Gamma_3 = \frac{\zeta}{2} \sqrt{7\chi/10} \ . \tag{4.3}$$

Notice that the effects associated with the Prandtl number do not appear in the final evolution equation. During the course of the derivation, we have implicitly made the assumption that P is at least an $O(1)$ quantity. In this case, because of symmetry with respect to the midplane of the liquid layer in the leading-order velocity boundary conditions, the terms multiplied by P^{-1} average to zero. However, the coefficient Γ_1 depends on the Prandtl number when there is asymmetry in the velocity boundary conditions at leading order in ϵ (see Chapman and Proctor [16]). When $P = O(\epsilon^2)$, the equations for ψ_0 and σ_0 are then coupled and their solution yields a nontrivial leading-order vorticity.

We observe that the symmetry-breaking mechanism in Eq. (3.28) is due to the solid layer thickness A and to the amount of interfacial deformations represented by the coefficients Γ_2 and Γ_3. Also note, from the problem formulation, that $A = 0$ implies zero deformations. However, it is possible for $A \neq 0$ and have zero deformations. In this case the solid layer plays the role of an upper planar plate that is less conducting than the original one.

We investigate the stability of the trivial solution of Eq. (4.2) by considering its linear version.

$$\frac{\partial F}{\partial w} + F_{\xi\xi\xi\xi} + 2F_{\xi\xi} + \hat{\beta}F = 0 \ . \tag{4.4a}$$

Equation (4.4a) admits solutions of the form

$$F(\xi, w) = \exp(aw + ib\xi) \ , \tag{4.4b}$$

where the growth rate a and the wave number b satisfy the dispersion relation

$$a = -(b^2 - 1)^2 + (1 - \hat{\beta}) \ . \tag{4.4c}$$

We notice from Eq. (4.4c) that $\hat{\beta} = 1$ is the critical value separating growing and decaying disturbances. The fastest growing disturbances have a wave number $b = 1$ (see Gertsberg and Sivashinsky [16]).

We consider the numerical solution of Eq. (4.2) with periodic boundary conditions on the interval $[0, 8\pi]$ by using a fully explicit finite-difference scheme. The interval of integration is divided into 300 mesh intervals, and the time step size Δw has been chosen to satisfy the stability criterion as given by the linear part of Eq. (4.2), $\Delta w \leq (\Delta\xi)^4/8$, where $\Delta\xi$ is the step size for ξ. The computations are then carried until a steady state is reached.

When solidification is absent, $A = 0$ and $\Gamma_3 = 0$, Eq. (4.2) reduces to the one derived by Knobloch [17]. It describes the time and spatial evolution of the leading-order concentration in the context of Soret-driven convection at positive separation ratio. The difference between his numerical coefficients and ours is due to the fact that his boundaries, which are impermeable, are located at $z = \pm 1$.

We find that the initial condition $F(\xi, 0) = 0.1\cos(\xi)$, converges to the trivial solution when $\hat{\beta} > 1$, but evolves toward a cellular state when $\hat{\beta} < 1$. The amplitude is found to increase with increases in the deviation of $\hat{\beta}$ from one, while the wavelength remains equal to the critical wavelength (see Fig. 2).

The presence of solidification, which is coupled to the interfacial deformations, Eq. (2.11b), affects the concentration profile in the liquid mixture. From the numerical solutions of Eq. (4.2), Figs. 3–5, we observe that increases in A lead to wider up-flow regions of warm fluid and narrower down-flow regions of cold fluid, and to a decrease in the amplitude of ϕ_0. This is an indication of broken up-down symmetry. Hadji and Schell [11] have indeed shown, by using a detailed small-amplitude stability analysis, that there exists a transition to subcritical down-hexagon patterns when $A > 0$. Similar observations have been made by Chapman and Proctor [16] when solving a nonlinear evolution equation for the leading-order convective temperature perturbation be-

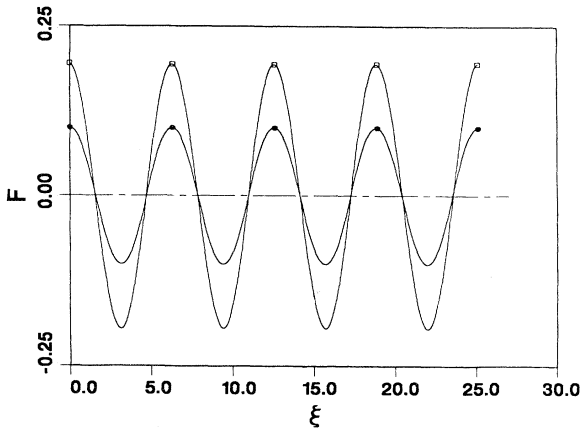

FIG. 2. Steady-state solution of Eq. (4.2) (□) for $\Gamma_1 = \Gamma_2 = \Gamma_3 = 0$. This corresponds to the *no-solidification case* with $A = 0$, $\hat{\beta} = 0.85$, $S = 0.01$, and $\tau = 0.01$. The initial condition $0.1\cos(\xi)$ is represented by (●).

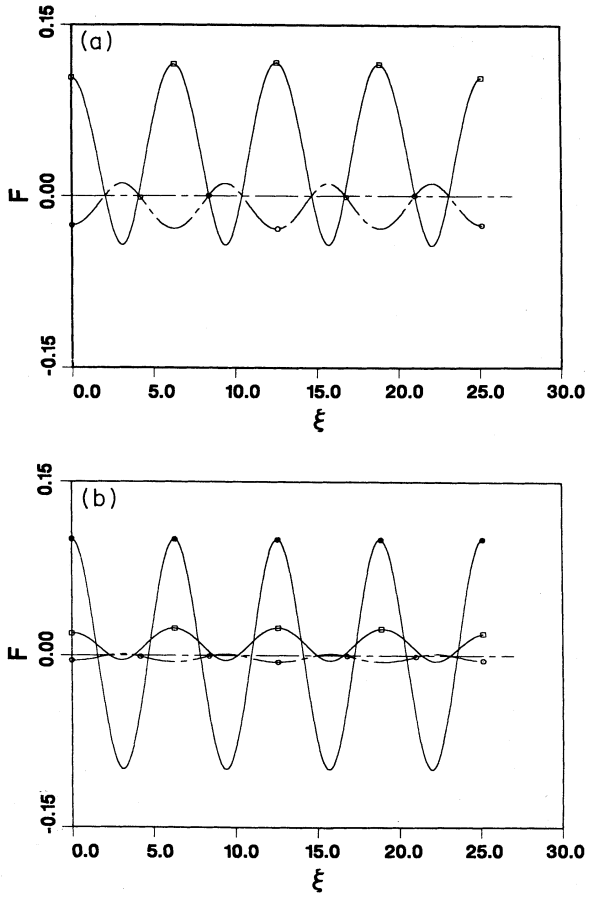

FIG. 3. Plots of the steady-state solution of Eq. (4.2) (□), and of the interfacial deformations, Eq. (3.30) (magnified by a factor of 25 for clarity), shown in (——○——) for $\hat{\beta}=0.85$, $S=0.01$, $\tau=0.01$, and $\zeta=0.5$; (a) $A=0.1$ and (b) $A=1.0$.

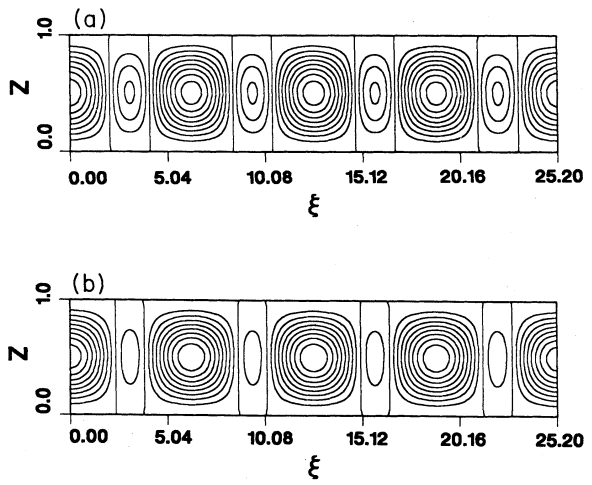

FIG. 4. Plot of ψ_0, Eq. (3.7), for parameters values $\hat{\beta}=0.85$, $\zeta=0.5$, $S=0.01$, and $\tau=0.01$ for (a) $A=0.1$ and (b) $A=1.0$. The wider cells correspond to warm up-flow and the narrow cells to cold down-flow.

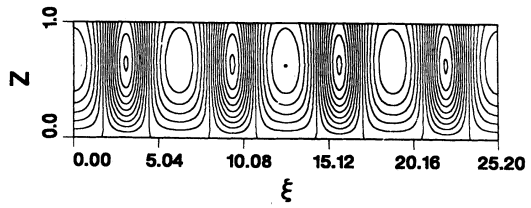

FIG. 5. Plot of Θ_2, Eq. (3.16), for the parameters values $A=0.1$, $\hat{\beta}=0.85$, $S=0.01$, $\zeta=0.5$, and $\tau=0.01$. The wider cells correspond to warm up-flow.

tween insulating boundaries. Their equation, which corresponds to Eq. (4.2) without the terms that are multiplied by Γ_2 and Γ_3, is solved numerically for the case of perfectly insulating plates, which corresponds to $\hat{\beta}=0$, and for an $O(1)$ deviation of the Rayleigh number from its critical value. Their plots show the same qualitative behavior as ours. Therefore these extra terms in front of Γ_2, and Γ_3 in Eq. (4.2), which owe their existence primarily to the deformations of the solid-liquid interface, do not seem to contribute to any new behavior. These coefficients are due solely to the amount of interfacial deformations and vanish for a planar interface. In all the

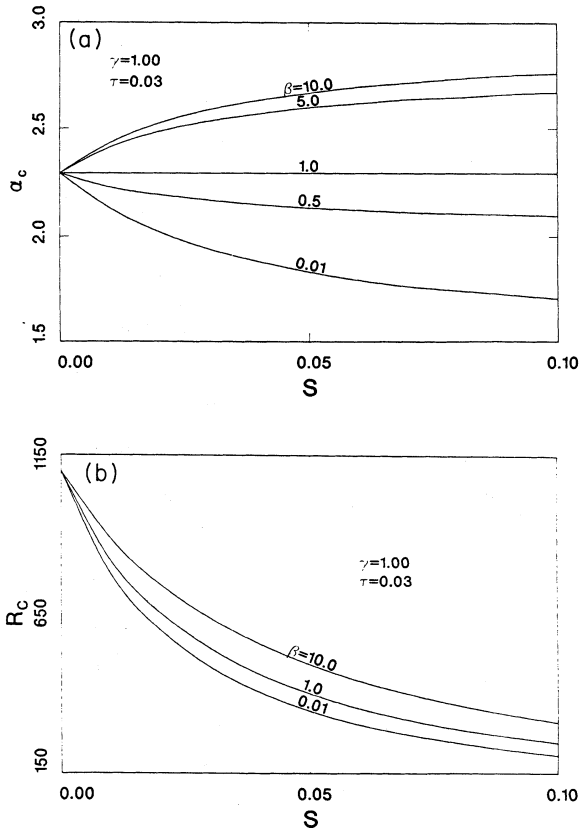

FIG. 6. Plots of (a) the critical wave number α_c and (b) the critical Rayleigh number R_c, for several values of the mass and heat transfer Biot numbers β and γ at the top and bottom boundaries, with Lewis number $\tau=0.03$ and solid layer thickness $A=0$.

cases that we have investigated, these interfacial deformations are found to have a much smaller amplitude than ϕ_0 to have any significant effects as long as $\zeta = O(1)$. We also observe that the nonplanar interface has a cellular structure that is identical in form to the convection pattern in the liquid.

V. CONCLUDING REMARKS

We have investigated the coupling between solidification and Soret-driven convection in a thin layer of a dilute binary mixture. Using a Bénard-like setup and a formulation that is in the spirit of Davis, Müller, and Dietsche [4], we were able to isolate the effects of the convective currents in the liquid, due to the Soret effect, on the shape of the solid-liquid interface. We have made some simplifying assumptions in order to keep the nonlinear analysis tractable. While most are standard approximations that are routinely made in solidification problems, the assumption of a planar interface in the static state requires some explanation. It is well known that during the freezing of a binary mixture, the solid-liquid interface may be subject to morphological instabilities that are of diffusive nature. Certain conditions on the interface velocity, the distribution coefficient, and the gradients of concentration and temperature must be met for the onset of this instability. In the limit of a vanishing interface velocity, the onset of the convective instability precedes the onset of the morphological instability [18]. Hence we have considered a situation in which the convective and morphological instabilities are effectively uncoupled. In this case the solid-liquid interface is planar and stationary in the conductive state, but deformable in the presence of convection.

The separation ratio S and the dimensionless thickness of the solid layer A are the most relevant parameters that appear in this problem. As in the case of solidification of a pure substance [4,5], the solidified layer plays the role of an upper deformable boundary that is impermeable to mass flow and is less conducting than the upper plate. The solutions of Eq. (4.2) indicate that the inclusion of δ in Eq. (3.30), by taking $\delta = O(\epsilon^2)$, has little effect on the profile of F or on the shape of the interface. Therefore the profile of η_2 is determined primarily by Θ_2. The dependence of η_2 on the concentration enters through the term $\nabla_H^2 F = \nabla_H^2 c_0$, since to leading order $\Theta_0 = 0$ and thus $F = c_0$.

If, instead of infinitely conducting plates, we consider plates that are poor conductors of heat compared to the fluid, then the problem must be reformulated to also include a heat-transfer Biot number γ at the lower plate. In this case, the critical wave number and the critical Rayleigh number for the onset of convection depend on γ and on the mass-transfer Biot number β. This dependence is shown in Figs. 6(a) and 6(b), for a Lewis number $\tau = 0.03$ and $A = 0$. Figure 6(a) shows plots of the critical wave number α_c against S for several values of β and γ. We note that α_c does not vary with S when γ and β are equal, but α_c decreases with increasing S for $\gamma > \beta$, and increases with increasing S for $\gamma < \beta$, i.e., the signs of $(\partial \alpha_c / \partial S)$ and $(\beta - \gamma)$ agree. We have also observed that the magnitude of α_c decreases in magnitude as both γ and β approach zero. Consequently, the lower bound on S, Eq. (3.28), for which these results are valid can be made smaller by considering plates which are poorer conductors of heat than the fluid. Thus a purely analytical weakly nonlinear pattern formation analysis, which includes transition from a thermally induced flow pattern $S = 0$ to a Soret-driven induced flow pattern $S > 0$ is plausible.

The critical Rayleigh number, however, decreases monotonically with the separation ratio S for any values of the Biot numbers β and γ. For S fixed, R_c is found to increase with increasing values of the difference $(\beta - \gamma)$; see Fig. 6(b).

[1] M. C. Dauzère, Ann. Phys. (Paris) **9**, 7 (1919), plates I–XII.

[2] H. Bénard, Rev. Gen. Sci. Pures Appl. **11**, 1261 1271 (1900); **11**, 1309 (1900).

[3] Up-hexagons are characterized by upwelled flow in the center, as opposed to down-hexagons that have downflow at their centers. Since the liquid was exposed to air during the cooling process, the hexagonal pattern observed by Dauzère, is most probably due the coupled effects of buoyancy and surface tension forces.

[4] S. H. Davis, U. Müller, and C. Dietsche, J. Fluid Mech. **144**, 133 (1984).

[5] C. Dietsche and U. Müller, J. Fluid Mech. **161**, 249 (1985).

[6] P. Bigazzi, S. Ciliberto, and V. Croquette, J. Phys. (Paris) **51**, 611 (1990); J. J. Niemela, G. Ahlers, and D. S. Cannel, Phys. Rev. Lett. **64**, 1365 (1990); K. D. Eaton, D. N. Ohlsen, S. Y. Yamamoto, C. M. Surko, W. Barten, M. Lücke, M. Kamps, and P. Kolodner, Phys. Rev. A **43**, 7105 (1991); B. L. Winkler and P. Kolodner, J. Fluid Mech. **240**, 31 (1992).

[7] E. Moses and V. Steinberg, Phys. Rev. A **43**, 707 (1991).

[8] T. Clune and E. Knobloch, Phys. Rev. A **44**, 8084 (1991).

[9] G. Zimmermann (unpublished).

[10] G. Zimmermann, U. Müller, and S. H. Davis, J. Fluid Mech. **238**, 657 (1992).

[11] L. Hadji and M. Schell, Phys. Fluids A **2**, 1597 (1990). Note that the expression for m should read $m = \delta K D_l / D_s$.

[12] L. Hadji and M. Schell, Phys. Fluids A **1**, 1467 (1989).

[13] J. K. Platten and J. C. Legros, *Convection in Liquids* (Springer-Verlag, Berlin, 1984); D. T. J. Hurle and E. Jakeman, J. Fluid Mech. **47**, 667 (1971).

[14] E. Knobloch and D. R. Moore, Phys. Rev. A **37**, 860 (1988).

[15] F. H. Busse and N. Riahi, J. Fluid Mech. **96**, 243 (1980).

[16] C. J. Chapman and M. R. E. Proctor, J. Fluid Mech. **101**, 759 (1980); M. R. E. Proctor, *ibid.* **113**, 469 (1981); V. Gertsberg and G. Sivashinsky, Prog. Theor. Phys. **66**, 1219 (1981); G. W. Young and S. H. Davis, Phys. Rev. B **34**, 3388 (1986).

[17] E. Knobloch, Phys. Rev. A **40**, 1549 (1989).

[18] S. R. Coriell, M. R. Cordes, W. J. Boettinger, and R. F. Sekerka, J. Cryst. Growth **49**, 13 (1980).